Chapter 15
Numerical Studies on the Reduced Order Modeling of Frictionless Joint Contact Interfaces

M. Breitfuss and H.J. Holl

Abstract This contribution focuses on the consideration of contact interface stresses within reduced order models of mechanical systems comprising frictionless lap joints. The reduced order models investigated are based on two types of extensions to the trial vector basis utilized in the fixed interface reduction method following Craig and Bampton.

After a short introduction the problem formulation, the motivation for investigating a frictionless contact interface and the according discretization for obtaining a numerical model are given. The zero thickness element based numerical model for the contact stresses within the frictionless joint contact interface is mentioned as well. This is followed by a recapitulation of the model order reduction process utilizing a Galerkin projection and referring to the reduction basis according to Craig and Bampton. The methods for obtaining the above mentioned extensions to this basis are outlined as well. Finally some meaningful results obtained from static and dynamic loading of the reduced order models are discussed. The respective numerical model represents a cantilever beam consisting of two solid metal components.

The methods are evaluated in terms of the required number of additional trial functions necessary for obtaining a satisfying approximation of the acting contact stresses. It turns out that one method allows for a lower number of trial functions while keeping accuracy at an very acceptable level.

Keywords Bolted connection • Contact interface • Model order reduction • Proper orthogonal decomposition • Zero thickness element

15.1 Introduction

The model order reduction of linear dynamic systems is state of the art. A well known approach for this kind of problems is the fixed interface reduction method following Craig and Bampton [3]. In contrast the model order reduction of systems involving nonlinearities, either local or globally distributed, is still under investigation. The reduced order modelling of mechanical structures comprising a joint, like a bolted connection, is such a demanding problem due to the nonlinear relations involved within the contact interface.

The method according to Craig and Bampton utilizes a set of trial vectors, which are used as approximation of the system displacement fields and as subspace where the resulting equation of motion gets projected on. An approach, which extends this set of trial vectors with an additional type of trial vectors for the local displacements within the contact interface, was proposed by [8]. Subsequent contributions [9], [10] and [11] further refined this approach.

The suggested set of trial vectors already lead to very promising results during own investigations of the authors. Within this contribution the convergence of the computed contact stresses is investigated. The explanation starts with the problem formulation and the discretization to obtain a numerical model. This is followed by a brief review of the Galerkin projection based model reduction approach. In this section the computation of the additional trial vector set according to [11] is given and followed by an approach, which is intended to deliver an "optimal" set of additional trial vectors. These two sets of trial vectors are evaluated in terms of accuracy of the contact stresses obtained from the reduced order model. Finally some conclusions are drawn from the numerical studies carried out.

M. Breitfuss (✉) • H.J. Holl
Johannes Kepler University Linz, Altenbergerstr. 69, 4040 Linz, Austria
e-mail: markus.breitfuss@jku.at

A. Brandt, R. Singhal (eds.), *Shock & Vibration, Aircraft/Aerospace, Energy Harvesting, Acoustics & Optics, Volume 9*,
Conference Proceedings of the Society for Experimental Mechanics Series, DOI 10.1007/978-3-319-30087-0_15

15.2 Problem Formulation

15.2.1 Governing Equations

The body Ω with the surface Γ comprising a contact interface Γ_{jc} as depicted in Fig. 15.1a is investigated. As boundary conditions the surface Γ_d is constrained and the stresses $\boldsymbol{t}_b$ on the surface Γ_t are prescribed. The surfaces Γ_d and Γ_t are disjunct surface regions of Γ. The dynamic equilibrium of a physical particle within the domain Ω at the position denoted by $\boldsymbol{x}$ is given by

$$\rho\ddot{\boldsymbol{u}} - div\boldsymbol{S} - \boldsymbol{k} = 0 \quad \forall \boldsymbol{x} \in \Omega \tag{15.1a}$$

with the boundary conditions

$$\boldsymbol{u} = 0 \quad \forall \boldsymbol{x} \in \Gamma_d \quad \text{and} \quad \boldsymbol{S}\boldsymbol{n} = \boldsymbol{t}_b \quad \forall \boldsymbol{x} \in \Gamma_t \tag{15.1b}$$

and the initial conditions for time $t = t_0 = 0$

$${}^0\boldsymbol{u} = \boldsymbol{u}_0 \quad \forall \boldsymbol{x} \in {}^0\Omega \quad \text{and} \quad {}^0\dot{\boldsymbol{u}} = \boldsymbol{v}_0 \quad \forall \boldsymbol{x} \in {}^0\Omega \tag{15.1c}$$

where ρ denotes the mass density, $\boldsymbol{u}$ the displacement, $\dot{\boldsymbol{u}} = \boldsymbol{v}$ the velocity, $\ddot{\boldsymbol{u}} = \boldsymbol{a}$ the acceleration, $\boldsymbol{S}$ the Cauchy stress tensor, $\boldsymbol{k}$ the imposed force density and $\boldsymbol{n}$ the surface normal pointing outwards. The left superscript ${}^0(.)$ is supposed to emphasize that a certain quantity (.) is evaluated at time t_0 or on the bodies initial configuration ${}^0\Omega = \Omega \times t_0$ respectively.

The body comprises a contact interface Γ_{jc} depicted in Fig. 15.1b. Contact stresses

$$\boldsymbol{S}^{\pm}\boldsymbol{n}^{\pm} = \boldsymbol{t}_{jc}^{\pm} \qquad \forall \boldsymbol{x} \in \Gamma_{jc} \tag{15.2}$$

will occur where $\boldsymbol{t}_{jc}^{\pm}$ denotes the acting joint contact stresses. The superscript $^{\pm}$ is used to denote that a certain quantity is related to the respective side of the contact interface.

To define the relations within the contact interface Γ_{jc} all physical particles P^- on the contact surface Γ_{jc}^- have to be related with the physical particles P^+ on Γ_{jc}^+. Once determined for the initial configuration all contact pairs $\{P^-, P^+\}$ remain associated due to the assumption of small relative displacement within the contact interface.

Utilizing the interface normal direction ${}^0\boldsymbol{n}_{jc} = {}^0\boldsymbol{n}^-$ one can define the gap function

$$g_n = [\boldsymbol{x}^+ - \boldsymbol{x}^-]^{T0}\boldsymbol{n}_{jc} \qquad \forall \boldsymbol{x} \in \Gamma_{jc} \tag{15.3}$$

which expresses the contact pair distance in contact interface normal direction. As the contact in surface normal direction is of main interest for the upcoming explanations the kinematics in contact surface tangential direction are not further discussed.

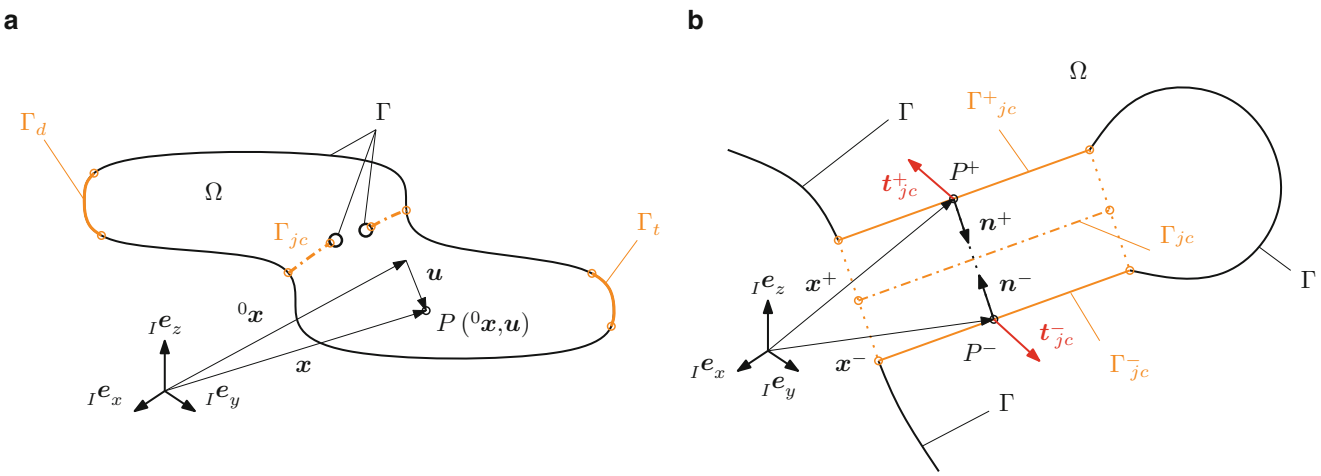

Fig. 15.1 Body Ω comprising a contact interface in actual configuration at time t (**a**) and contact stresses within the contact interface Γ_{jc} for the contact pair $\{P^-, P^+\}$ (**b**)

The occurring contact stresses for a contact pair $\{P^-, P^+\}$, arbitrarily selected from the currently contacting ($\boldsymbol{t}_{jc} \neq 0$) sub domain of the contact interface Γ_{jc} are, according to Newton's 3rd Law, equal in magnitude but acting in opposing directions

$$\boldsymbol{t}_{jc} = \boldsymbol{t}_{jc}^{-} = -\boldsymbol{t}_{jc}^{+} \qquad \forall \boldsymbol{x} \in \Gamma_{jc}. \tag{15.4}$$

The contact interface stress vector can be separated into two components

$$\boldsymbol{t}_{jc} = \boldsymbol{t}_n + \boldsymbol{t}_t \tag{15.5}$$

where $\boldsymbol{t}_n$ is defined to point in contact interface normal direction and the remaining part $\boldsymbol{t}_t$ is oriented tangential to the contact surface.

The latter component is neglected as this contribution focuses on the computation of the stress component in normal direction. The energy dissipation due to friction within the contact interface will not be investigated. However it is required to suppress the tangential relative movement of the contact partners, at least to obtain a correct global behaviour of the body. This can be achieved by a permanent tangential coupling of the contact partners within a small area of the contact interface. This small area is assumed to permanently comprise a sufficiently high contact stress normal component due to the bolt pretension. This finally leads to a contact stress vector

$$\boldsymbol{t}_{jc} = \boldsymbol{t}_n = t_n \boldsymbol{n}_{jc}. \tag{15.6}$$

where t_n denotes the scalar valued contact stress component in interface normal direction.

Utilizing the gap function g_n and the contact stress component t_n one can finally formulate the nonlinear contact conditions of the frictionless contact interface Γ_{jc}

$$g_n \geq 0, \quad t_n \leq 0, \quad g_n t_n = 0 \qquad \forall \boldsymbol{x} \in \Gamma_{jc}. \tag{15.7}$$

15.2.2 Discretization

For the whole body domain Ω a linear constitutive law without rate dependencies is assumed and the occurring displacements $\boldsymbol{u}$ are expected to be small compared to the body dimensions. From the virtual displacements denoted by $\delta\boldsymbol{u}$, which are presumed to be small in relation to the body dimension as well, one can derive the virtual strain tensor $\delta\boldsymbol{\epsilon}$. Utilizing the principle of virtual work one obtains the weak formulation of the dynamic equilibrium

$$\delta W_\Omega + \delta W_{\Gamma_{jc}} = 0 \tag{15.8a}$$

where the virtual work of the body domain Ω reads

$$\delta W_\Omega = \int_\Omega \rho \ddot{\boldsymbol{u}} \cdot \delta \boldsymbol{u} \; d\Omega + \int_\Omega \boldsymbol{S} : \delta \boldsymbol{\epsilon} \; d\Omega - \int_{\Gamma_t} \boldsymbol{S}\boldsymbol{n} \cdot \delta \boldsymbol{u} \; d\Gamma - \int_\Omega \boldsymbol{k} \cdot \delta \boldsymbol{u} \; d\Omega \tag{15.8b}$$

and the virtual work of the contact interface domain Γ_{jc} is given by

$$\delta W_{\Gamma_{jc}} = -\int_{\Gamma_{jc}^-} \boldsymbol{t}_{jc}^- \cdot \delta \boldsymbol{u}^- d\Gamma - \int_{\Gamma_{jc}^+} \boldsymbol{t}_{jc}^+ \cdot \delta \boldsymbol{u}^+ d\Gamma. \tag{15.8c}$$

Both quantities, Eqs. (15.8b) and (15.8c), are treated separately.

15.2.2.1 Body Domain

The body domain ${}^0\Omega$ is discretized with the finite element discretization $\widehat{\Omega}$ comprising the node locations $\widehat{\boldsymbol{x}}$ and the elements $\widehat{\Omega}^{(e)} \subset \widehat{\Omega}$. The discretization of the surface regions Γ_d and Γ_t are denoted by $\widehat{\Gamma}_d$ and $\widehat{\Gamma}_t$ respectively. Based on the interpolation of the displacement field within the domain of each element e, given by

$$u^{(e)} \approx N^{(e)}\, \widehat{u}^{(e)}, \tag{15.9}$$

where $\boldsymbol{N}^{(e)}$ holds the shape functions of the respective element formulation and $\widehat{\boldsymbol{u}}(e)$ denotes the nodal degrees of freedom of all nodes connected to the element, one can evaluate the integrals in Eq. (15.8b) using a numerical integration scheme. It is assumed that the prescribed displacement boundary conditions are directly incorporated into the principle of virtual work, see e.g. [1] or [12] for a detailed description. Performing these tasks leads to the linear, undamped equation of motion without contact consideration

$$\boldsymbol{M}\ddot{\widehat{\boldsymbol{u}}} + \boldsymbol{K}\widehat{\boldsymbol{u}} = \boldsymbol{f}_e \tag{15.10}$$

where $\boldsymbol{M}$ denotes the mass matrix and $\boldsymbol{K}$ denotes the stiffness matrix of the constrained system. Displacements and accelerations of each node are collected in $\widehat{\boldsymbol{u}}$ and $\ddot{\widehat{\boldsymbol{u}}}$ respectively. The vector of external forces $\boldsymbol{f}_e$ considers both the prescribed stresses $\boldsymbol{t}_b$ and the imposed force density $\boldsymbol{k}$.

15.2.2.2 Contact Interface Domain

The contact interface domain is discretized utilizing zero thickness elements which implement a penalty approach for regularization of the contact interface conditions Eq. (15.7). In this case the finite element discretization $\widehat{\Omega}$ is required to comprise a matching mesh of all element surfaces adjacent to the contact interface. Then the discretization $\widehat{\Gamma}_{jc}$ of the joint contact interface Γ_{jc} is obtained by a composition of zero thickness elements $\widehat{\Gamma}_{jc}^{(e)}$ where one surface connects to a single element belonging to $\widehat{\Gamma}_{jc}^{-}$ and the other surface to a single element part of $\widehat{\Gamma}_{jc}^{+}$.

Formulations for obtaining a zero thickness element related contribution to the stiffness matrix $\Delta\boldsymbol{K}_{jc} \equiv \Delta\boldsymbol{K}_{jc}(\widehat{\boldsymbol{u}})$ can be found in literature, e.g [4] or [6]. In case of reduced order modeling, e.g. using a Galerkin projection based approach, the authors suggest a formulation which contributes to the nodal force vector on the right hand side of Eq. (15.10). Such an approach is outlined in [2] where the formulation of a 3 (6) node zero thickness element is provided as well. For easier reference the contact stress equivalent nodal force vector of the zero thickness element is given in a slightly modified writing

$$\boldsymbol{f}_{jc}^{(e)} = \int_{\widehat{\Gamma}_{jc}^{(e)}} [\boldsymbol{N}^{(e)} - \boldsymbol{N}^{(e)}]^T\, \boldsymbol{t}_{jc}^{(e)}\, d\widehat{\Gamma}. \tag{15.11}$$

$\boldsymbol{N}^{(e)}$ denotes the matrix of element shape functions and $\widehat{\Gamma}_{jc}^{(e)}$ denotes the domain of the respective zero thickness element surface. The contact stress component is computed via the "constitutive" relation

$$t_n = \begin{cases} 0 & \text{if} \quad g_n \geq 0, \\ c_n g_n & \text{if} \quad g_n < 0 \end{cases}. \tag{15.12}$$

with the penalty parameter c_n. The resulting nonlinear equation of motion with contact consideration is given by

$$\boldsymbol{M}\ddot{\widehat{u}} + \boldsymbol{K}\widehat{u} = f_e + f_{jc}. \tag{15.13}$$

where $\boldsymbol{f}_{jc}$ denotes the contact stress equivalent nodal force vector representing all zero thickness elements. The quantity $\boldsymbol{f}_{jc}$ is formally obtained utilizing the linear assembly Operator A on the nodal force vectors of each zero thickness element

$$\boldsymbol{f}_{jc} = \underset{\widehat{\Gamma}_{jc}}{A}\, \boldsymbol{f}_{jc}^{(e)}. \tag{15.14}$$

15.3 Model Order Reduction

15.3.1 Basics

It is assumed that an approximation of the nodal displacements $\widehat{\boldsymbol{u}}$ in Eq. (15.13) is given by the Ritz ansatz

$$\widehat{\boldsymbol{u}} \approx \boldsymbol{\Phi}\boldsymbol{q} \tag{15.15}$$

with the mode matrix $\boldsymbol{\Phi}$ which columnwise holds the displacement trial vectors $\boldsymbol{\varphi}_i$ and the according generalized coordinates $\boldsymbol{q}$. If the number of generalized coordinates $\boldsymbol{q}$ is significantly smaller than the dimension of $\widehat{\boldsymbol{u}}$ the mode matrix $\boldsymbol{\Phi}$ can be utilized as reduction basis to obtain a reduced order model.

Substituting the ansatz Eq. (15.15) into Eq. (15.13) and performing a Galerking projection by premultiplying the resulting equation with $\boldsymbol{\Phi}^T$ finally leads to the reduced equation of motion

$$\boldsymbol{M}_{red}\ddot{\boldsymbol{q}} + \boldsymbol{K}_{red}\boldsymbol{q} = \boldsymbol{f}_{red} + \boldsymbol{\Phi}^T\boldsymbol{f}_{jc} \tag{15.16}$$

where $\boldsymbol{M}_{red} = \boldsymbol{\Phi}^T\boldsymbol{M}\boldsymbol{\Phi}$ denotes the reduced mass matrix, $\boldsymbol{K}_{red} = \boldsymbol{\Phi}^T\boldsymbol{K}\boldsymbol{\Phi}$ denotes the reduced stiffness matrix and $\boldsymbol{f}_{red} = \boldsymbol{\Phi}^T\boldsymbol{f}_e$ denotes the projected vector of external forces.

An reduced order model is intended to approximate a high dimensional solution space by a lower dimensional solution space with acceptable tradeoff in accuracy. One has to keep in mind that the solution obtained from such a reduced order model is constrained to the low dimensional solution space spanned by the trial vectors $\boldsymbol{\Phi}$. Therefore a proper trial vector basis is crucial for obtaining a satisfactory reduced order model.

For this sake the vector of nodal displacements is partitioned

$$\widehat{\boldsymbol{u}} = \begin{bmatrix} \widehat{\boldsymbol{u}}_i \\ \widehat{\boldsymbol{u}}_b \end{bmatrix} \tag{15.17}$$

where $\widehat{\boldsymbol{u}}_i$ denotes the displacement of the inner degrees of freedom and $\widehat{\boldsymbol{u}}_b$ denotes the displacement of the n_b boundary degrees of freedom within the discretized surfaces $\widehat{\Gamma}_d$ and $\widehat{\Gamma}_t$. Appropriate trial vectors for the investigation of the vibrational behavior of a linear mechanical system (up to a certain frequency limit) are suggested in [3]. With the help of these trial vectors one can construct a mode basis

$$\boldsymbol{\Phi}_{classic} = [\boldsymbol{\Psi}_c \boldsymbol{\Phi}_n] \tag{15.18}$$

which holds n_b constraint modes $\boldsymbol{\Psi}_c$ and n_n fixed interface normal modes $\boldsymbol{\Phi}_n$. The computation of these two types of trial vectors is described in detail in [3].

Unless a very high number of trial vectors is considered this mode basis does not guarantee to accurately capture the local displacements within the contact interface. As consequence the computed contact stresses might not be sufficiently accurate as well. To overcome this limitation [8] proposed to extend an existing mode base, like the above mentioned classic mode basis following Craig and Bampton, by a set of so called joint interface modes $\boldsymbol{\Phi}_{jim}$. These modes account for the local displacements due to the contact interface. Furthermore Newtons 3rd law is explicitly considered within their formulation.

Methods for the computation are given in [8], [9] and [11], the resulting extended transformation matrix reads

$$\boldsymbol{\Phi} = [\boldsymbol{\Psi}_c \;\; \boldsymbol{\Phi}_n \;\; \boldsymbol{\Phi}_{jim}]. \tag{15.19}$$

15.3.2 Brief Review on Proper Orthogonal Decomposition

The Proper Orthogonal Decomposition (POD) is a method for extracting the essential information out of a given collection of k snapshots $\boldsymbol{y}_j$. This essential information is expressed by a low dimensional set of $\ell < k$ basis vectors $\boldsymbol{v}_i$ which approximate the collection of snapshots in an optimal sense, see [7]. These POD basis vectors are a solution to the minimization problem

$$\min_{v_1,\ldots,v_\ell} \sum_{j=1}^{k} \left\| y_j - \sum_{i=1}^{\ell} \left\langle y_j, v_i \right\rangle_W v_i \right\|^2 \tag{15.20a}$$

so that

$$\left\langle v_i, v_j \right\rangle_W = \delta_{ij} \qquad \text{for} \quad i,j = 1, \ldots, \ell \tag{15.20b}$$

where

$$\langle \boldsymbol{a}, \boldsymbol{b} \rangle_W = \langle \boldsymbol{a}, \boldsymbol{W}\boldsymbol{b} \rangle = \langle \boldsymbol{W}\boldsymbol{a}, \boldsymbol{b} \rangle = a^T \boldsymbol{W}\boldsymbol{b} \tag{15.21}$$

denotes the weighted inner product of two vectors with a positive definite weighting matrix $\boldsymbol{W}$. A basis $\boldsymbol{V} = [\boldsymbol{v}_1, \ldots, \boldsymbol{v}_\ell]$, which is a solution to the above minimization problem, can be obtained by solving the symmetric eigenvalue problem

$$\boldsymbol{Y}^T \boldsymbol{W} \boldsymbol{Y} \bar{\boldsymbol{v}}_i = \lambda_i \boldsymbol{v}_i \qquad \text{for} \quad i = 1, \ldots, \ell \tag{15.22a}$$

where $\boldsymbol{Y} = [\boldsymbol{y}_1, \ldots, \boldsymbol{y}_k]$. The final POD basis vectors are obtained by evaluating

$$\boldsymbol{v}_i = \frac{1}{\sqrt{\lambda_i}} \boldsymbol{Y} \bar{\boldsymbol{v}}_i. \qquad \text{for} \quad i = 1, \ldots, \ell \tag{15.22b}$$

This procedure is sometimes called the method of snapshots [7].

15.3.3 Test Load Based Joint Interface Modes

In [11] it was suggested to define test loads within the contact interface and utilize the POD on the resulting displacement fields for computation of the joint interface modes. The respective steps are briefly recalled in this subsection.

First step is the decomposition of the discretized contact interface $\widehat{\Gamma}_{jc}$ into n subareas as suggested in [9]. Each of these subareas is loaded by a unit pressure distribution, according to Newton's 3rd law on both sides $^{\pm}$ of the contact interface. The resulting equivalent nodal force vectors are collected in the matrix of test loadcases

$$\boldsymbol{F}_{jc}^{(*)} = \left[f_{jc,1}^{(*)}, \ldots, f_{jc,n}^{(*)} \right]. \tag{15.23}$$

These test load cases are utilized within the static equilibrium

$$\boldsymbol{K} \widehat{U}^{(*)} = \boldsymbol{F}_{spc} + \boldsymbol{F}_{jc}^{(*)} \tag{15.24}$$

where the body is fixed at $\widehat{\Gamma}_d$ and $\widehat{\Gamma}_t$ as well. The constraints at $\widehat{\Gamma}_d$ are already considered within the principle of virtual work, the constraints at $\widehat{\Gamma}_t$ are enforced by the respective column vectors of the matrix $\boldsymbol{F}_{spc}$. The resulting displacement fields are collected in the matrix $\widehat{U}^{(*)} = \left[\widehat{u}_1^{(*)}, \ldots, \widehat{u}_n^{(*)} \right]$.

By setting $\boldsymbol{Y} = \widehat{U}^{(*)}$ and $\boldsymbol{W} = \boldsymbol{I}$ the application of the snapshot method Eq. (15.22) for computation of the joint interface modes $\boldsymbol{\Phi}_{jim}^{A} = \boldsymbol{V}$ is pretty straight forward.

Furthermore [11] suggests to use the stiffness matrix for weighting, $\boldsymbol{W} = \boldsymbol{K}$, which lead to promising results during own investigations of the authors. This requires a positive definite stiffness matrix, which is ensured in our case as $\boldsymbol{K}$ represents the constrained body. This method will be denoted as "method A" for the remainder of this contribution.

15.3.4 Contact Simulation Based Joint Interface Modes

To improve the convergence of the computed contact stresses with respect to the required number of joint interface modes the authors propose to utilize the contact forces resulting from selected contact simulations for the computation of joint interface modes. These contact simulations, which comprise static and dynamic loadcases, are presented in this subsection.

15.3.4.1 Static Loadcases

By means of the partitioning scheme introduced in Eq. (15.17) the static equilibrium equation of the body fixed at $\widehat{\Gamma}_d$ is given by

$$\boldsymbol{K}\widehat{\boldsymbol{u}}(s) = \begin{bmatrix} \boldsymbol{K}_{ii} & \boldsymbol{K}_{ib} \\ \boldsymbol{K}_{bi} & \boldsymbol{K}_{bb} \end{bmatrix} \begin{bmatrix} \widehat{\boldsymbol{u}}_i(s) \\ \widehat{\boldsymbol{u}}_b(s) \end{bmatrix} = \boldsymbol{f}_e^{(s)} + \boldsymbol{f}_{jc}^{(s)} = \begin{bmatrix} \boldsymbol{0}_{ie} \\ \boldsymbol{f}_{be}^{(s)} \end{bmatrix} + \begin{bmatrix} \boldsymbol{f}_{ijc}^{(s)} \\ \boldsymbol{0}_{bjc} \end{bmatrix} \tag{15.25}$$

The k nodal contact force $f_{jc,j}^{(s)}$ snapshots due to different external force vectors $\boldsymbol{f}_{e,j}^{(s)}$ are collected in the matrix

$$\boldsymbol{F}_{jc}^{(s)} = [\boldsymbol{f}_{jc,1}^{(s)}, \ldots, \boldsymbol{f}_{jc,k}^{(s)}] \tag{15.26}$$

for subsequent processing. It is worth to note that, due to the nonlinear relations within the contact interface, superposition is not possible any longer. For this reason the external force vectors $\boldsymbol{f}_{e,j}^{(s)}$ need to comprise meaningful load combinations covering each boundary degree of freedom.

15.3.4.2 Dynamic Loadcases

By means of the partitioning scheme introduced in Eq. (15.17) the initial value problem of the body fixed at $\widehat{\Gamma}_d$ is given by the equation of motion

$$\boldsymbol{M}\ddot{\widehat{\boldsymbol{u}}}^{(d)} + \boldsymbol{K}\widehat{\boldsymbol{u}}(d) = \begin{bmatrix} \boldsymbol{M}_{ii} & \boldsymbol{M}_{ib} \\ \boldsymbol{M}_{bi} & \boldsymbol{M}_{bb} \end{bmatrix} \begin{bmatrix} \ddot{\widehat{\boldsymbol{u}}}_i^{(d)} \\ \ddot{\widehat{\boldsymbol{u}}}_b^{(d)} \end{bmatrix} + \begin{bmatrix} \boldsymbol{K}_{ii} & \boldsymbol{K}_{ib} \\ \boldsymbol{K}_{bi} & \boldsymbol{K}_{bb} \end{bmatrix} \begin{bmatrix} \widehat{\boldsymbol{u}}_i(d) \\ \widehat{\boldsymbol{u}}_b(d) \end{bmatrix} = \boldsymbol{f}_e^{(d)} + \boldsymbol{f}_{jc}^{(d)} = \begin{bmatrix} \boldsymbol{0}_{ie} \\ \boldsymbol{f}_{be}^{(d)} \end{bmatrix} + \begin{bmatrix} \boldsymbol{f}_{ijc}^{(d)} \\ \boldsymbol{0}_{bjc} \end{bmatrix}. \tag{15.27a}$$

with the initial conditions

$${}^0\widehat{\boldsymbol{u}}(d) = \boldsymbol{u}_0 \quad \forall \widehat{\boldsymbol{x}} \in \widehat{\Omega} \qquad \text{and} \qquad {}^0\dot{\widehat{\boldsymbol{u}}}^{(d)} = \boldsymbol{0} \quad \forall \widehat{\boldsymbol{x}} \in \widehat{\Omega}. \tag{15.27b}$$

The initial displacement is either intended to consider the prestressed state due to pretension of the bolted connection or simply $\boldsymbol{u}_0 = \boldsymbol{0}$. To obtain stable responses, independently from the respective numerical time integration scheme, some damping should be introduced into the equation of motion. The authors suggest to utilize a Rayleigh damping approach where the damping matrix is a linear combination of mass and stiffness matrix. This is feasible as the main purpose of the simulations is to obtain meaningful snapshots due to the evolvement of the inner degrees of freedom resulting from the dynamic excitation of the boundary degrees of freedom.

The suggested k excitations are formally given by

$$\boldsymbol{f}_{e,j}^{(d)} = \begin{cases} \boldsymbol{0} & t \leq 0 \\ \boldsymbol{f}_{e,j}^{(s)} & t > 0 \end{cases} \qquad \text{for} \quad j = 1, \ldots, k \tag{15.28}$$

where $\boldsymbol{f}_{e,j}^{(s)}$ corresponds to the static loadcases investigated in Sect. 15.3.4.1. The response to each of these k excitations, up to at least one period of the dominant vibration, is computed. To lower the computational burden a prior model reduction step, e.g. [5], is highly recommended.

The time discretized evolvement of the jth solution leads to n_j nodal contact force $\boldsymbol{f}_{jc,i}^{(d,j)}$ snapshots which are collected in the matrix

$$\boldsymbol{F}_{jc}^{(d,j)} = [\boldsymbol{f}_{jc,1}^{(d,j)}, \ldots, \boldsymbol{f}_{jc,n_j}^{(d,j)}] \tag{15.29}$$

for subsequent processing.

15.3.4.3 Trial Vectors

To compute the trial vectors all contact force snapshots Eqs. (15.26) and (15.29) are combined in a single matrix

$$\boldsymbol{F}_{jc}^{(sd)} = [\boldsymbol{F}_{jc}^{(s)}, \boldsymbol{F}_{jc}^{(d,1)}, \ldots, \boldsymbol{F}_{jc}^{(d,k)}]. \tag{15.30}$$

By setting $\boldsymbol{Y} = \boldsymbol{F}_{jc}^{(sd)}$ and $\boldsymbol{W} = \boldsymbol{I}$ the application of the snapshot method Eq. (15.22) again is pretty straight forward. Finally the resulting contact force vectors $\boldsymbol{F}_{jim} = \boldsymbol{V}$ are utilized within the static equilibrium Eq. (15.24). The resulting displacement shapes already represent the vector space of the suggested joint interface modes $\boldsymbol{\Phi}_{jim}^{B}$.

This method will be denoted as "method B" for the remainder of this contribution.

15.4 Numerical Example

15.4.1 Model Description

The reference method Sect. 15.3.3 and the proposed method Sect. 15.3.4 for computation of the joint interface modes are applied to the finite element model of a bolted cantilever beam depicted in Fig. 15.2.

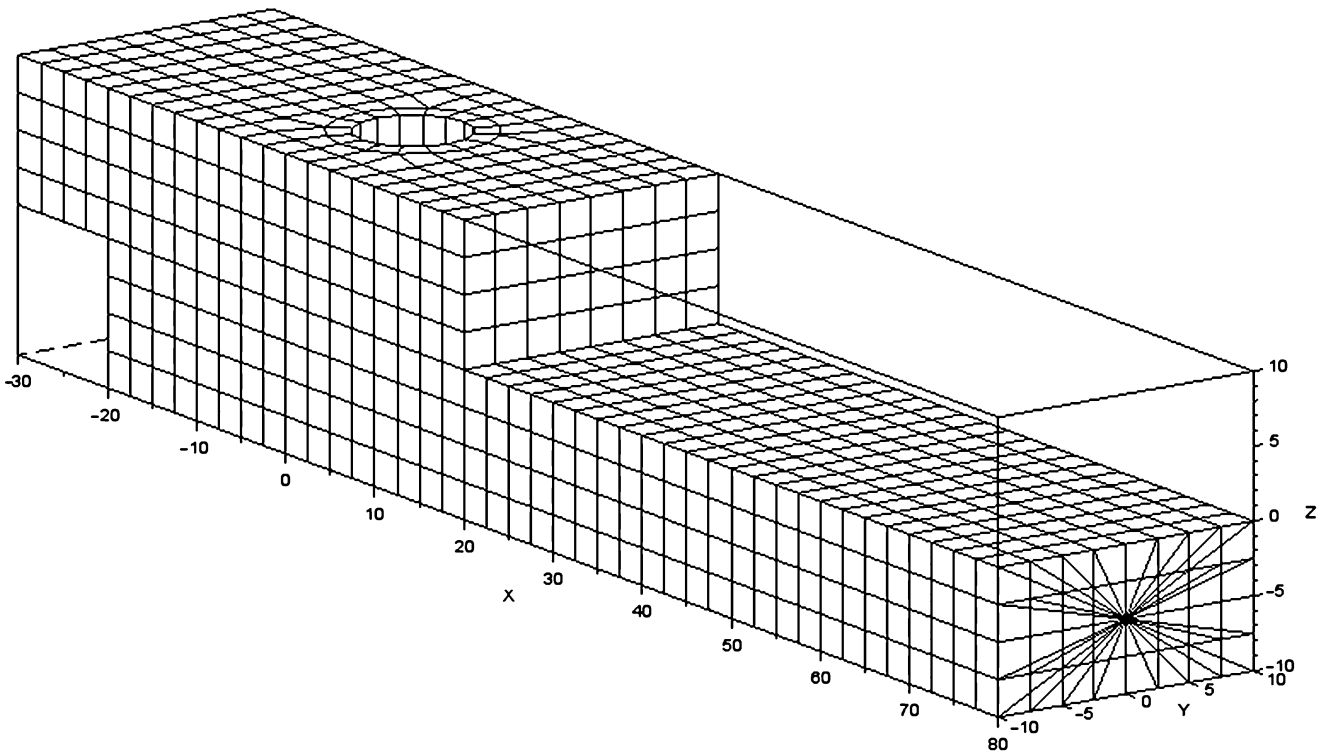

Fig. 15.2 Finite element model of the bolted cantilever (the beam element based bolt model is hidden)

The body consists of two substructures with rectangular shaped cross section ($a = 10$ mm, $b = 20$ mm) and an overall length of $l = 110$ mm. The substructures are connected by a contact interface and a single bolt. All structural components are modeled using a linear elastic material with Young's Modulus $E = 210{,}000$ N/mm^2, Poisson ratio $\nu = 0.29$ and density $\rho = 7820$ kg/m^3.

The discretization $\widehat{\Omega}$ of the full model comprises 1834 elements and 2780 nodes. The CHEXA, CBEAM, RBE2 and RBE3 element formulations of the commercial FEM software package MSC Nastran are used to generate the system matrizes within Eq. (15.10). The contact interface $\widehat{\Gamma}_{jc}$ is discretized with an 4 (8) node zero thickness element formulation which allows to obtain the contact stress equivalent nodal force vector within Eq. (15.13).

A convergence study regarding the meshsize of the full model is not within the scope of this contribution. It is assumed that the accuracy of the contact stresses obtained from this numeric model are sufficiently accurate for the purpose of this model. The purpose of the reduced order model is to reproduce these contact stresses with sufficiently low error but significantly higher computational efficiency.

15.4.2 Sticking Friction Definition

During generation of the system matrices using a commercial FEM software package there is no connection of the two contacting substructures except the beam element based bolt model. The resulting Eq. (15.13) is utilized for a contact simulation where the structure is constrained at $\widehat{\Gamma}_d$ and the bolt is incrementally pretensioned to a nominal value. The resulting contact stresses are depicted on the left hand side of Fig. 15.3.

All contact node pairs possessing a contact pressure over a certain threshold are assumed to stick together in tangential direction during all subsequent simulations. The node pairs selected this way are marked on the right hand side of Fig. 15.3. The sticking friction condition within this area is approximated utilizing a penalty approach. All subsequent steps consider these additional penalty stiffness related entries in the stiffness matrix.

15.4.3 Reduction Basis

The computation of static and dynamic loadcases to generate snapshots for obtaining a reduction basis was carried out according to Sect. 15.3.4. The static loadcases represent load combinations of bolt pretension, vertical tip load and torsional moment at the free end of the cantilever.

The dynamic loadcases, computed with a nominal pretension of the bolt, are limited to combinations of vertical load and torsional moment at the free end of the cantilever. For easier computation the equation of motion comprises an additional Rayleigh approach based damping matrix. The step responses are obtained from the equation of motion, which is transformed to a system of first order differential equations, utilizing the implizit Euler integration scheme.

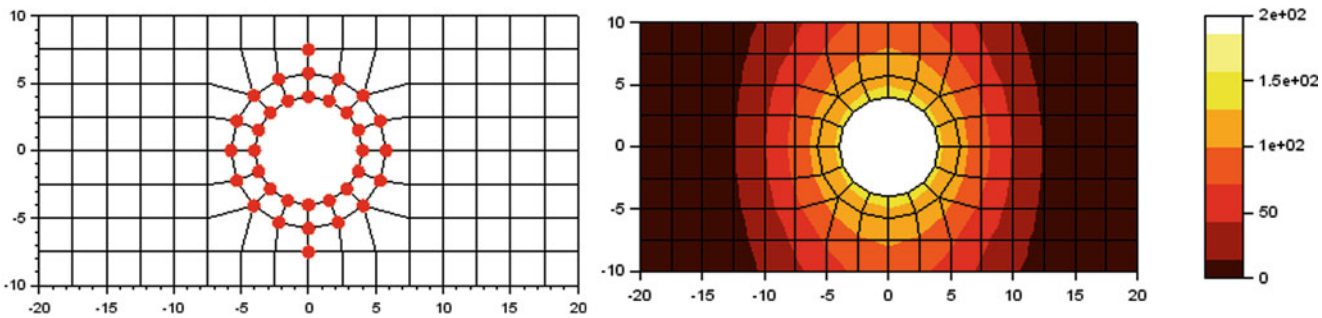

Fig. 15.3 Contact stresses in surface normal direction resulting from a nominal pretension of the bolted joint (*left*). Locations with sticking friction are identified based on a contact stress threshold. To suppress the tangential relative movement of the adjoining contact node pairs a penalty approach is utilized at the marked node pairs (*right*)

15.4.4 Contact Stress Accuracy Evaluation

15.4.4.1 Static Loadcases

Two exemplary loadcases are documented within this section. The first loadcase denoted as *LC*1 is a vertical tip load while the second loadcase denoted as *LC*2 additionally comprises a torsional moment. It is noted that both loadcases are not explicitly considered as certain load combination during computation of the snapshots for obtaining the reduction basis (Fig. 15.4).

The according contact pressure distributions in surface normal direction are depicted in Fig. 15.5.

The relative error of the contact stresses in surface normal direction is chosen as evaluation criteria. This quantity illustrates whether the computed contact stresses are useful for subsequent computations, e.g. for the computation of shear stresses due to friction. For a vector $\boldsymbol{y}$ the relative error vector is given by

$$e_{rel} = \frac{\boldsymbol{y} - y_{ref}}{\|y_{ref}\|_{\infty}} \tag{15.31}$$

where $\|.\|_{\infty}$ denotes the maximum norm of a vector and $\boldsymbol{y}_{ref}$ denotes the reference values obtained from the full model. For computation of the contact pressure relative error the maximum contact pressure value of the reference solution is used as reference value.

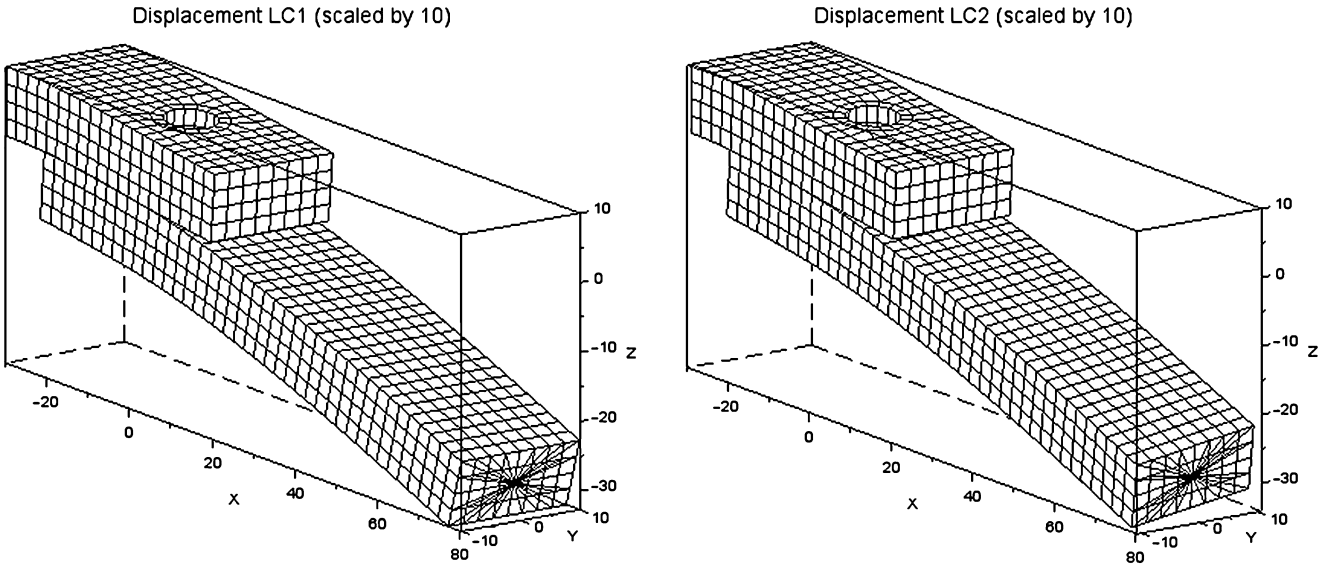

Fig. 15.4 Resulting displacement of the two substructures for *LC*1 (*left*) and *LC*2 (*right*)

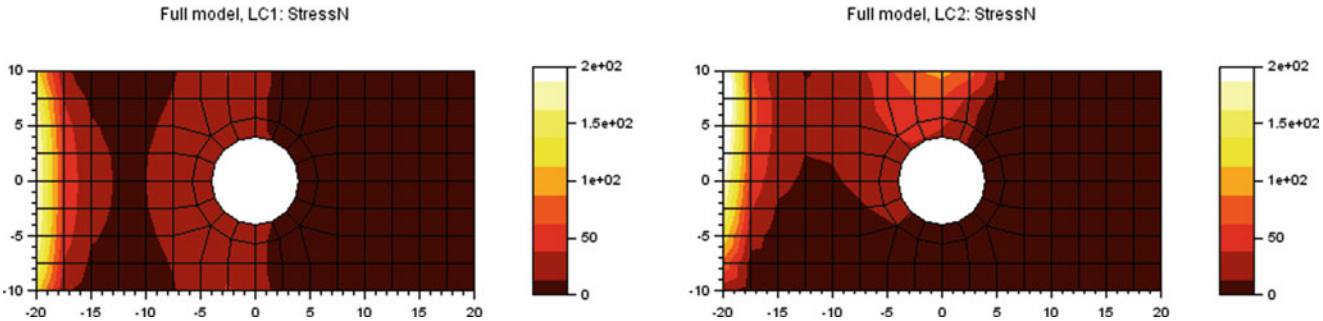

Fig. 15.5 Contact pressure obtained from the full model for loadcase LC1 (*left*) and loadcase LC2 (*right*)

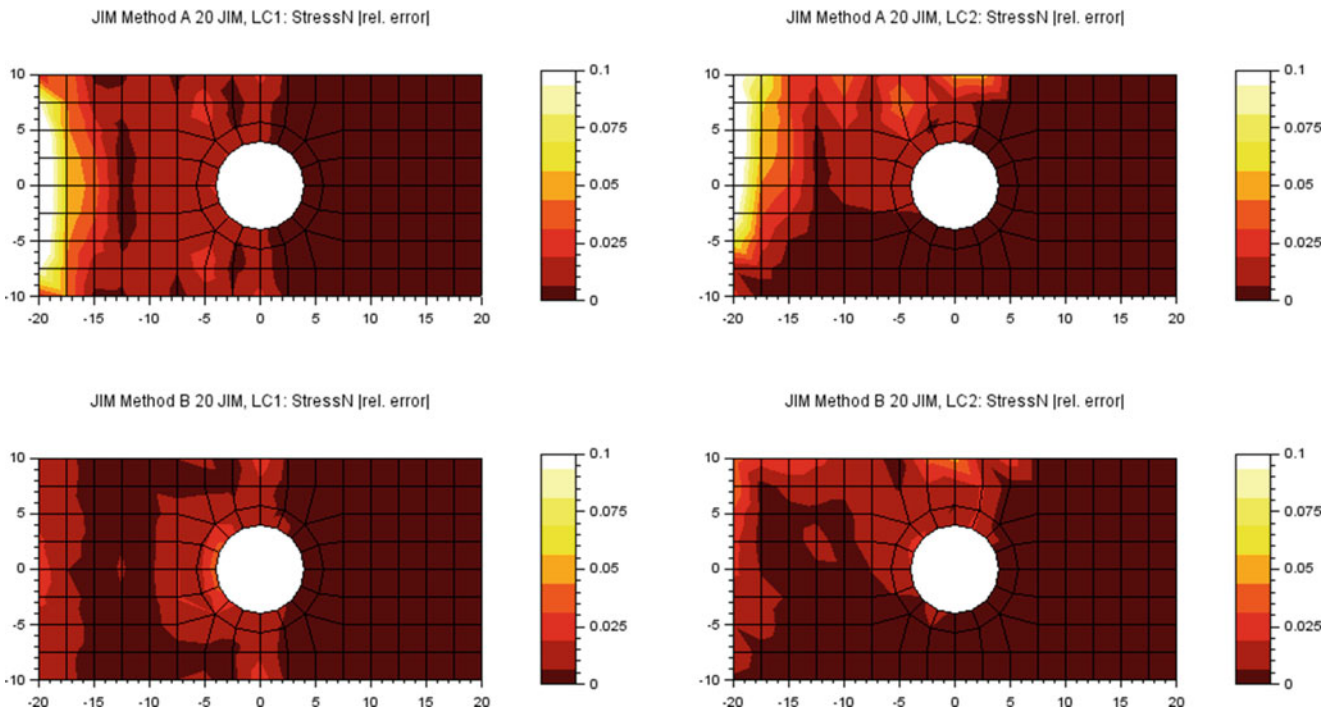

Fig. 15.6 Relative error of the contact pressure obtained from the reduced order model with method A based joint interface modes (*top row*) and method B based joint interface modes (*bottom row*)

The respective error distributions for the reduced order models are depicted in Fig. 15.6. The following conclusions can be drawn:

- Symmetric contact pressure distributions lead to symmetric error distributions.
- The maximum relative error is significantly larger than 10 % when utilizing 20 JIMs obtained by method A
- The maximum relative error is less than 5 % when utilizing 20 JIMs obtained by method B.

It can be noted that further investigations indicate a more rapid convergence rate of the joint interface modes computed by method B than those computed by method A.

15.4.4.2 Dynamic Loadcase

The response of the cantilevers free end due to LC2 applied as a step function is depicted in Fig. 15.7. Already five joint interface modes, either computed using method A or method B, are sufficient to resemble the cantilevers free end displacement of the reference solution. Evaluation of the maximum contact pressure leads to a different conclusion:

- Method A based JIMs lead to a significantly higher maximum contact pressure.
- Method B based JIMs almost resemble the maximum contact pressure of the reference solution.

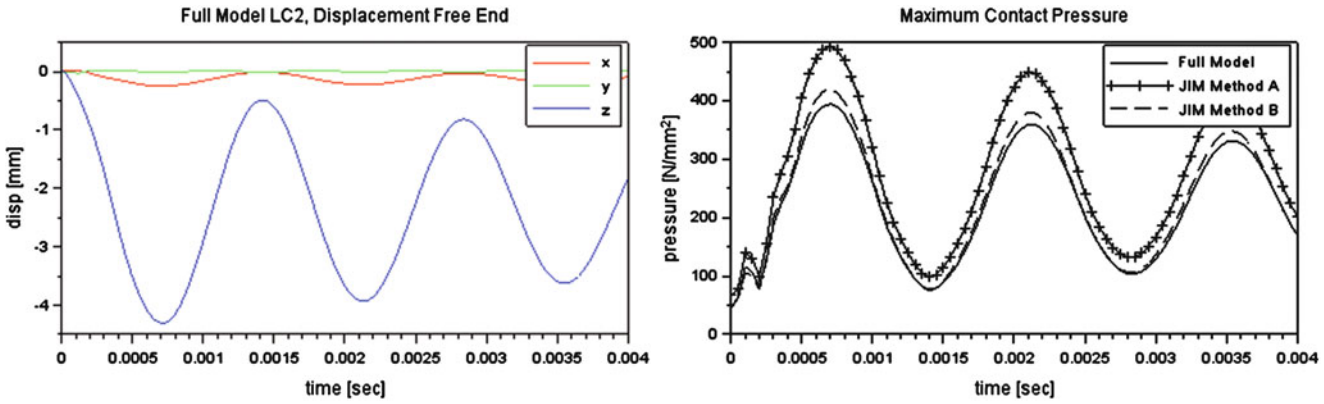

Fig. 15.7 Vibration due to an stepwise excitation with the load combination of LC2: displacement of the free end (*left*) and maximum contact pressure (*right*)

15.5 Conclusion

The numerical example reveals that an POD reduction basis obtained from a methodical defined collection of contact simulation based snapshots is superior to an reduction basis obtained from snapshots based on test loads within the investigated contact interface. This conclusion is based on the relative error of the contact stresses computed utilizing the according reduced order models with respect to the contact stresses obtained from the full model.

But it has to be noted that the test load based reduction basis can be obtained with reasonable effort while the computational burden involved to realize the contact simulations quickly gets tremendous, especially for complex structures comprising many boundary degrees of freedom. Therefore the results suggest the existence of an optimal basis of trial vectors for contact interfaces, but an efficient approach for obtaining such a basis still has to be found.

Acknowledgements Support of the authors by the K2 Austria Center of Competence in Mechatronics (ACCM) and the Engineering Center Steyr (MAGNA) is gratefully acknowledged.

References

1. Bathe, K.-L.: Finite Element Procedures. Prentice Hall, Upper Saddle River (1996)
2. Breitfuss, M., Irschik, H., Holl, H.J., Witteveen, W.: DEIM for the efficient computation of contact interface stresses. In: Allen, M., Mayes, R., Rixen, D. (eds.) Proceedings of the 32nd IMAC, A Conference and Exposition on Structural Dynamics, 2014. Conference Proceedings of the Society for Experimental Mechanics Series, vol. 1, pp. 435–445. Springer, New York (2014)
3. Craig, R.R., Bampton, M.C.C.: Coupling of substructures for dynamic analyses. AIAA J. **6**(7), 1313–1319 (1968)
4. Mayer, M.H., Gaul, L.: Segment-to-segment contact elements for modelling joint interfaces in finite element analysis. Mech. Syst. Signal Process. **21**(2), 724 – 734 (2007)
5. Qu, Z.-Q.: Model reduction for dynamical systems with local nonlinearities. AIAA J. **40**(2), 327–333 (2002)
6. Süß, D., Willner, K.: Investigation of a jointed friction oscillator using the multiharmonic balance method. Mech. Syst. Signal Process. **52–53**, 73 – 87 (2015)
7. Volkwein, S.: Model reduction using proper orthogonal decomposition. http://www.math.uni-konstanz.de/numerik/personen/volkwein/teaching/POD-Vorlesung.pdf (September 2014)
8. Witteveen, W., Irschik, H.: Efficient modal formulation for vibration analysis of solid structures with bolted joints. In: Conference Proceedings of IMAC-XXV: A Conference & Exposition on Structural Dynamics, Orlando, 19–22 February 2007
9. Witteveen, W., Irschik, H.: Efficient computation of joint interface modes. In: Proceedings of the IMAC-XXVII, Orlando, 9–12 February 2009
10. Witteveen, W., Irschik, H.: Efficient mode based computational approach for jointed structures: joint interface modes. AIAA J. **47**(1), 252–263 (2009)
11. Witteveen, W., Sherif, K.: Pod based computation of joint interface modes. In: Proulx, T. (ed.) Linking Models and Experiments. Conference Proceedings of the Society for Experimental Mechanics Series, vol. 2, pp. 19–28. Springer, New York (2011)
12. Zienkiewicz, O.C., Taylor, R.L., Zhu, J.Z.: The Finite Element Method: Its Basis and Fundamentals, 7th edn. Butterworth-Heinemann, Oxford (2013)